


ARTICLE

Cumulative deamidations of the major lens protein γ S-crystallin increase its aggregation during unfolding and oxidation

Calvin J. Vetter¹ | David C. Thorn² | Samuel G. Wheeler¹ |
 Charlie C. Mundorff^{3,4} | Kate A. Halverson³ | Thomas E. Wales⁴ |
 Ujwal P. Shinde³ | John R. Engen⁴ | Larry L. David³ | John A. Carver² |
 Kirsten J. Lampi¹ 

¹Integrative Biosciences, Oregon Health & Science University, Portland, Oregon

²Research School of Chemistry, College of Science, The Australian National University, Acton, Australia

³Chemical Physiology & Biochemistry, Oregon Health & Science University, Portland, Oregon

⁴Department of Chemistry & Chemical Biology, Northeastern University, Boston, Massachusetts

Correspondence

John A. Carver, Research School of Chemistry, College of Science, The Australian National University, Acton, ACT 2601, Australia.
 Email: john.carver@anu.edu.au

Kirsten J. Lampi, Integrative Biosciences, Oregon Health & Science University, 3181 SW Sam Jackson Park Road, Portland, OR 97239-3098.
 Email: lampik@ohsu.edu

Funding information

Australian National Health and Medical Research Council, Grant/Award Number: 1068087; National Eye Institute, Grant/Award Numbers: EY010572, EY027012, EY027768; NIH Office of the Director, Grant/Award Number: OD012246; Northeastern University, Grant/Award Number: student fellowship

Abstract

Age-related lens cataract is the major cause of blindness worldwide. The mechanisms whereby crystallins, the predominant lens proteins, assemble into large aggregates that scatter light within the lens, and cause cataract, are poorly understood. Due to the lack of protein turnover in the lens, crystallins are long-lived. A major crystallin, γ S, is heavily modified by deamidation, in particular at surface-exposed N14, N76, and N143 to introduce negative charges. In this present study, deamidated γ S was mimicked by mutation with aspartate at these sites and the effect on biophysical properties of γ S was assessed via dynamic light scattering, chemical and thermal denaturation, hydrogen-deuterium exchange, and susceptibility to disulfide cross-linking. Compared with wild type γ S, a small population of each deamidated mutant aggregated rapidly into large, light-scattering species that contributed significantly to the total scattering. Under partially denaturing conditions in guanidine hydrochloride or elevated temperature, deamidation led to more rapid unfolding and aggregation and increased susceptibility to oxidation. The triple mutant was further destabilized, suggesting that the effects of deamidation were cumulative. Molecular dynamics simulations predicted that deamidation augments the conformational dynamics of γ S. We suggest that these perturbations disrupt the native disulfide arrangement of γ S and promote the formation of disulfide-linked aggregates. The lens-specific chaperone α A-crystallin was poor at preventing the aggregation of the triple mutant. It is concluded that surface

Abbreviations: %Pd, polydispersity; C-td, C-terminal domain; DLS, SLS, and MALS, dynamic, static, and multi-angle light scattering; DTT, dithiothreitol; GuHCl, guanidine hydrochloride; HDX, hydrogen-deuterium exchange; N-td, N-terminal domain; SDS-PAGE, sodium dodecyl sulfate-polyacrylamide gel electrophoresis; TCEP, Tris(2-carboxyethyl)phosphine hydrochloride; TM, triple mutant; WT, wild type.

deamidations cause minimal structural disruption individually, but cumulatively they progressively destabilize γ S-crystallin leading to unfolding and aggregation, as occurs in aged and cataractous lenses.

KEYWORDS

cataracts, crystallins, deamidation, dynamic and static light scattering, hydrogen-deuterium exchange, mass spectrometry, oxidation, protein aggregation, protein unfolding

1 | INTRODUCTION

In mammals, the eye lens plays a crucial role in vision via transmitting, refracting, and focusing light onto the retina. Lens functionality is maintained via a high concentration of crystallin proteins (up to 300–500 mg/ml in the center of the lens) that are arranged in a supramolecular array with short-range order.¹ The lens is a unique organ in that it has no blood supply and there is no protein turnover in its fiber cells because they lack the organelles for protein synthesis and degradation. As a result, crystallins are long-lived proteins.² Cataract arises from opacification and concomitant light scattering associated with the unfolding, aggregation and precipitation of crystallins. Cataract is the major cause of blindness in the world and is the leading cause of low vision in the United States.³ Age-related cataract is the most prevalent type although many crystallin mutations give rise to congenital and early-onset cataract. The molecular mechanism(s) whereby cumulative modifications of crystallins lead to the formation of large, light scattering aggregates in the aging lens is poorly understood. A major contributing factor to this obscurity is the complexity of the insoluble aggregates isolated from human lenses.^{4–9}

There are three types of mammalian crystallins, α , β/γ , which are all comprised of a variety of isoforms. The two α -crystallins (A and B) are small heat-shock molecular chaperone proteins.^{10,11} The β/γ -crystallin family members are homologous to each other and are not related to the α -crystallins. The β/γ -crystallins are β -sheet-rich, two-domain proteins with the β -sheets adopting a Greek key arrangement. The Greek key motif contains four β -strands. In γ S-crystallin (γ S), the predominant γ -crystallin produced postnatally, each domain comprises two Greek key motifs, that is, a total of eight β -strands (Figure 1).¹² The γ -crystallins are primarily monomeric with their domains linked by a connecting peptide that is bent whereas in β -crystallins the connecting peptide is either bent or extended leading to oligomer formation with hydrophobic interactions stabilizing the interface between the domains.^{13–16}

The β/γ -crystallins comprise approximately two-thirds of the protein content of the human lens by mass and are extensively modified.^{17,18} Due to the absence of protein turnover, the lens is an incubator that accumulates multiple crystallin modifications over the individual's lifetime. Deamidation is a major age-related modification associated with *in vivo* insolubilization of crystallins.^{6,19–21} Deamidation of substantially buried residues in β/γ -crystallins induces significant destabilization.^{22–28} The most prevalent *in vivo* deamidation sites in the β/γ -crystallins, however, are in solvent-exposed regions.^{6,29,30} For example, human γ S undergoes significant deamidation with age, in this case the conversion of asparaginyl (Asn) residues, principally at surface residues (N14, N76, and N143), each to four possible isomers of

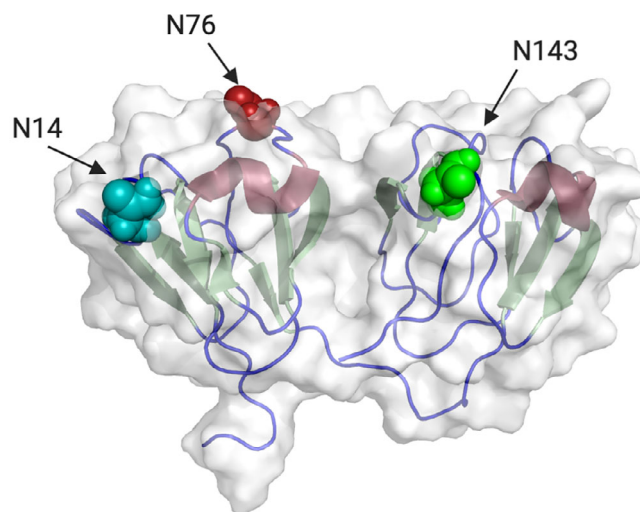


FIGURE 1 Solution structure of human γ S showing the location of Asn residues 14, 76, and 143. Deamidation was mimicked at Asn residues 14 (teal), 76 (firebrick red), and 143 (green). Asparagine residues 14 and 76 are located on the surface of the N-terminal domain (N-td) and residue 143 is on the surface of the C-terminal domain (C-td). Residues of interest are shown in spheres. Gray area represents solvent accessibility, green arrows represent β -sheets and red ribbons represent α -helices as generated with PyMol (Schrodinger, Inc. New York, NY). (PDB: 2M3T)

aspartic acid, that is, L-Asp, L-isoAsp, D-Asp and D-isoAsp.^{21,31,32} The modification levels in aged γ S range from 25–60% at N14, 50–80% at N76, and 20–90% at N143.^{6,21,29,30,33,34} These levels of deamidation correlate with their surface accessibility, that is, the labile polar Asn residues at positions 14, 76, and 143, have solvent exposures of \sim 55, 58, and 60%, respectively.^{35,36} Their location is indicated on the solution NMR-derived structure of γ S in Figure 1.¹² The level of γ S with in vivo deamidations at all three sites is estimated to be about 30% based on our recently published data for deamidation at N14 (84%) and N76 (73%) and on previous reports for deamidation at N143 (about 50%).^{29,37} The extent of deamidation in the entire crystallin mixture, including these three surface sites in γ S, is significantly greater in cataractous lenses compared with age-matched, non-cataractous controls, and significantly greater in the insoluble fraction than the soluble fraction of these lenses, implying that these modifications contribute to cataract formation.^{6,21,29,33,34}

Previous studies have investigated the effects of deamidation of γ S by mimicking deamidated residues with L-Asp, replacing L-Asn via mutagenesis and introducing a negative charge at the site of modification. Deamidation at N76 and N143 leads to increased attraction between monomers⁷ and even to dimer formation in the absence of reducing agent.³⁸ Further, we recently reported that single-point deamidations on the surface of the N-terminal domain (N-td) of γ S can alter its conformational dynamics, providing a potential mechanism for the aggregation and insolubilization of deamidated crystallins in the eye lens.³⁷ In this present study, the effect of deamidation (conversion to L-Asp) at each of these three sites (N14D, N76D, and N143D), along with the triple mutant (TM), was investigated to determine how specific surface deamidations on γ S could increase aggregation without significantly altering the global conformation of γ S and if a potential mechanism involved the stability and unfolding properties of γ S. We report the novel finding that deamidated γ S is more susceptible to intermolecular disulfide bonding and aggregates into larger light scattering bodies under physiologically relevant conditions. A possible mechanism is identified under partially denaturing and oxidative conditions, where the deamidation mimics undergo more rapid unfolding and aggregation, particularly N76D, compared with wild type (WT) γ S. TM γ S is further destabilized, illustrating the effects of successive deamidation as occurs in the lens with age. Furthermore, the lens-specific molecular chaperone α A-crystallin is relatively ineffective at acting as a chaperone to prevent the aggregation of destabilized TM γ S. It is concluded that surface

deamidations, while causing minimal structural disruption individually, progressively destabilize γ S and potentially other crystallins, leading to their unfolding and precipitation in aged and cataractous lenses.

2 | RESULTS

2.1 | Aggregation of human wild type and deamidated γ S under native conditions

Surface deamidation of γ S increased its propensity to form large aggregates that were detected by dynamic light scattering (DLS). Freshly prepared WT γ S (at 1 mg/ml) showed a predominant single peak containing 93% of the total light scattering intensity with a mean hydrodynamic radius (R_h) of 2.5 nm (ranging from 1.5–4.9 nm with 19% polydispersity [%Pd]) and a smaller amount of scattering due to a species between 10 and 100 nm in the intensity distribution (Figure 2, Table 1). The former is consistent with literature R_h values of 2.0–2.5 nm for monomeric γ S.^{39,40} At a higher concentration of 5 mg/ml, a similar R_h was detected for the main peak with significantly less %Pd (9%), but a greater amount of the larger species was detected plus an additional species with a R_h of >100 nm (Figure 2, Table 1).

In contrast to WT γ S, the deamidation mimics showed predominantly two to three distinct peaks with a greater fraction of DLS intensity due to the peaks of larger radius and less due to the main peak (peak 1) comprising the monomer. Peak 1 of the deamidation mimics had a mean R_h ranging from 2.7 to 3.3 nm (Table 1); while not significantly different from the WT γ S, the N14D and N76D mimics' peak 1 had a wider size distribution, ranging from 1.5–9.9 nm and significantly greater %Pd (35–37% compared with 19% for WT). Peak 2, with R_h values ranging from 10 to 100 nm, contributed 14–57% to the overall light scattering in the mimics compared with only 7% in WT γ S at the same concentration of 1 mg/ml. In N143D and TM γ S, peak 3, with R_h values between 200 and 400 nm, contributed 6–13% of the total light scattering.

The wider distribution of R_h and greater %Pd of the deamidated mimics N14D and N76D suggested greater size heterogeneity, indicating the presence of dimers or other species larger than a monomer even in peak 1 (Table 1). All of the mimics had relatively more light scattering from larger species than WT γ S, with N143D and the TM showing additional, even larger species. In summary, a small number of large light scattering aggregates were detected in DLS peaks in the deamidation mimics that were not present in WT γ S.

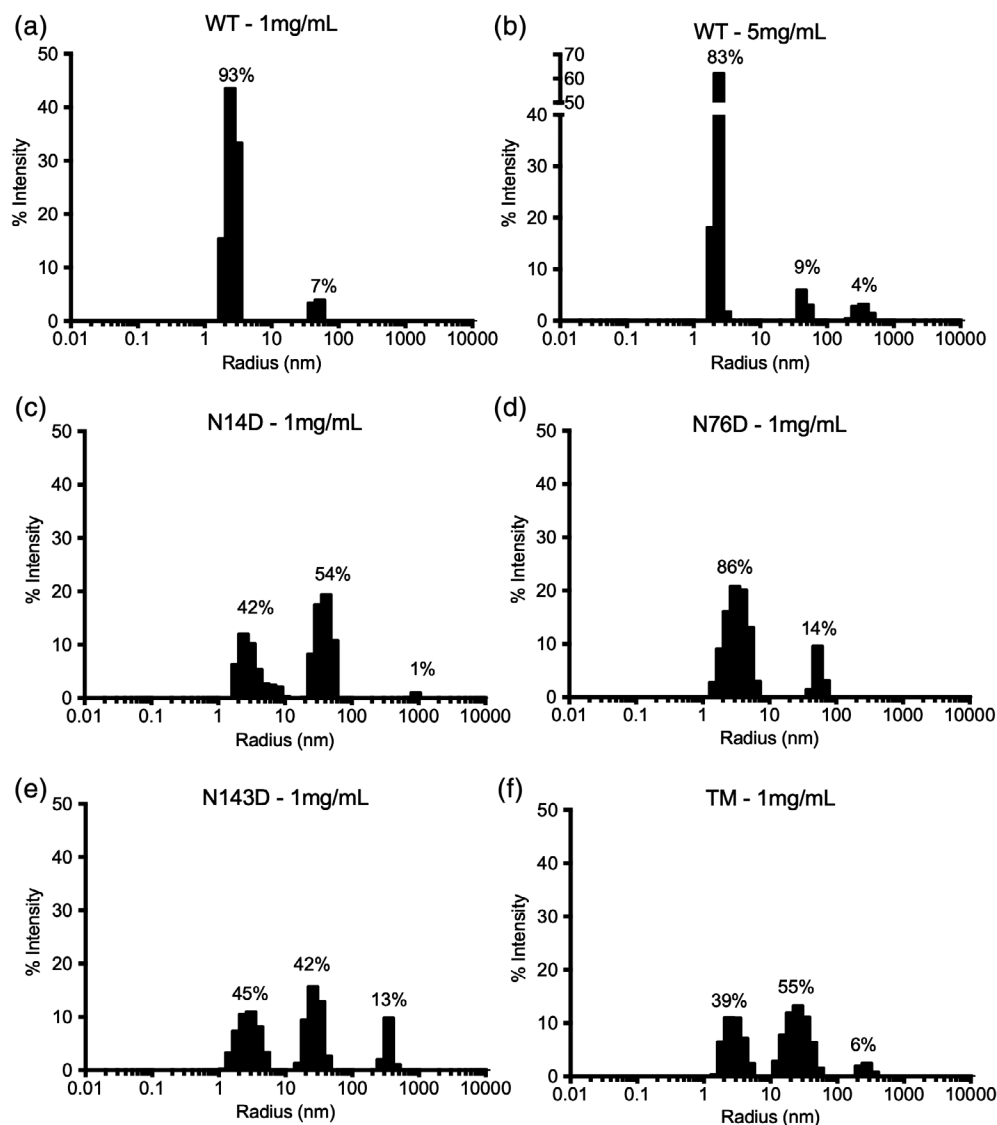


FIGURE 2 DLS measurements of the R_h distributions of γ S and deamidated mutants under native conditions. The intensity of DLS (% Intensity) derived from regularization analysis was plotted as a function of R_h with R_h values binned to 1–10 nm (peak 1), 10–100 nm (peak 2), and 100–1,000 nm (peak 3). (a and b) The % Intensity of WT species at 1 mg/ml and 5 mg/ml respectively. (c–f) The % Intensity of N14D, N76D, N143D and TM γ S at 1 mg/ml. Data were collected at 25°C. Data are representative of three independent experiments

TABLE 1 Sizes of γ S in Peak 1 determined by DLS

γ S	Concentration	Radius (nm)	% Pd
	mg/ml	Mean (SEM)	Mean (SEM)
WT	1	2.5 (0.2)	19 (4)
	5	2.4 (0.2)	6* (2)
N14D	1	3.2 (0.5)	37* (6)
N76D	1	3.3 (0.3)	35* (3)
N143D	1	2.7 (0.2)	29 (2)
TM	1	2.9 (0.3)	22 (4)

Note: The hydrodynamic radius and % polydispersity (% Pd) of γ S in peak 1 (1–10 nm) from Figure 2. Significant differences in % Pd between WT (1 mg/ml) and deamidated γ S were determined using a Student's *t* test are denoted with $p \leq .05$ (*), $n = 3$ –5.

2.2 | The molecular weight of wild type and deamidated γ S under native conditions

The formation of larger light scattering species by the deamidation mimics was confirmed by SEC-MALS comparing WT and TM γ S (Figure 3). Both proteins eluted primarily as a monomer at 14.5 ml with a M_w of 20.5×10^3 ($\pm 0.2\%$) g/mol, comparable to the predicted M_w of 20.9×10^3 g/mol (Figure 3a, blue arrow). Protein eluting in the monomer peak was homogeneous (polydispersity index of 1.000). In addition to the monomer peak, WT and TM γ S exhibited an early eluting peak at 7.5 ml, overlapping with the void peak at 7 ml. This early peak was of much higher intensity in TM compared with WT γ S.

The monomer peaks of WT and TM γ S shown in Figure 3a were collected and their homogeneity verified

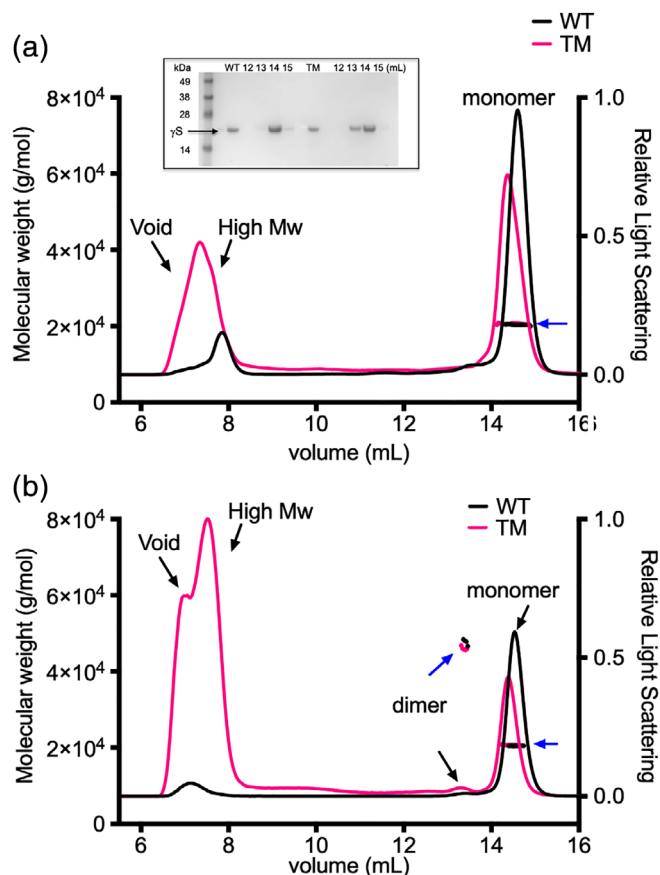


FIGURE 3 Molecular weight of γ S and triply deamidated mutant (TM) under native conditions. Multi-angle static light scattering (MALS) of WT and TM γ S was measured in-line with size exclusion chromatography (SEC-MALS). The right axis is relative Rayleigh LS of WT (black line) and TM (magenta line). The left axis is the weight average molecular weight (noted by a blue arrow). (a) Analysis of freshly prepared WT and TM γ S. Monomer peaks eluted at 14.5 ml and high M_w peaks eluted at 7.5 ml. The M_w for the monomer peaks was $20.5 \times 10^3 (\pm 0.2)$ g/mol (blue arrow) compared with the predicted M_w of 20.9×10^3 . Inset: SDS-PAGE analysis of chromatography fractions. Lane 1 contains molecular weight markers. Lanes 2 and 7 contain 2.5 μ g of unfractionated WT γ S-crystallin and TM proteins, respectively. Lanes 3–6 contain fractions of WT γ S, 12–15 ml. Lanes 8–10 contain fractions of TM γ S, 12–15 ml. (b) Analysis of incubated WT and TM γ S monomers. The monomer peaks isolated in panel A were incubated at 37°C for 6 days and then reanalyzed by SEC-MALS. Monomer peaks were detected with M_w of $20.6 \times 10^3 (\pm 0.2)$ g/mol (right blue arrow) and dimer peaks eluted at 13.5 ml with a M_w of $46.8 \times 10^3 (\pm 1.2)$ g/mol (left blue arrow). The high M_w peak for the TM in panel B was estimated to range from $3\text{--}9 \times 10^6$ g/mol (off scale)

by SDS-PAGE (Figure 3a inset). The fractions containing the monomer peaks of each protein were pooled and incubated at 37°C for 6 days before re-examination by SEC-MALS (Figure 3b). Incubating TM and, to a lesser degree, WT, generated a monomer peak with a similar

molecular weight (Figure 3b, right blue arrow), plus a minor light scattering peak at 13.5 ml with a M_w of $46.8 \times 10^3 (\pm 1.2\%)$ g/mol, corresponding to the approximate molecular weight of a γ S dimer (Figure 3b, left blue arrow). Moreover, the relative light scattering peak between 6 and 8 ml increased in proportion to the monomer peak in the case of TM γ S, suggesting the early eluting peak was due to large oligomers formed by monomers during incubation. In the case of WT γ S, an increase in the height of the early eluting peak was not observed.

The high molecular weight peak of TM γ S had a M_w of $3\text{--}9 \times 10^6$ g/mol and contained 0.8% of the total protein. In the case of WT γ S, the amount of protein in this peak was too low for M_w determination. Peaks were confirmed by mass spectrometry to contain γ S (Figure S1). Hence, under native conditions, TM γ S more heavily favored a small population of conformer that was aggregation-prone.

2.3 | Detection of partially unfolded intermediates of wild type and deamidated γ S during chemical unfolding

Equilibrium unfolding experiments were first performed to measure the thermodynamic stability of deamidated γ S relative to WT γ S. There are two tryptophan (Trp) residues in the N-td and two in the C-td of γ S. The location of these Trp residues permits their use as probes of the global structure.⁴¹ The Trps were selectively excited and their fluorescence measured in the presence of increasing concentrations of the denaturant, guanidine hydrochloride (GuHCl). The unfolding transition of WT was best fitted to a two-state model (native and unfolded) as has previously been reported^{42,43} with a midpoint of unfolding (C_M) of 2.6 M and an apparent Gibbs free energy of unfolding, ΔG°_{N-U} , of 12.0 ± 0.9 kcal/mol (Figure S2), comparable to previously published values.^{42,43} The unfolding transitions of the deamidated γ S variants were 2.5–2.6 M GuHCl deviating only marginally from that of WT γ S, and the Gibbs free energy of unfolding was slightly less than that of WT between 8.1 and 10.4 kcal/mol (Figure S2).

In order to further probe the tendency of γ S to aggregate, proteins were unfolded in 2.75 M GuHCl, near the concentration of half-equilibrium unfolding. Following different times of GuHCl exposure, they were subjected to pulse labeling in hydrogen-deuterium exchange (HDX) D_2O buffer to measure the number of solvent exposed amides (Figure 4). Three distinct major mass species were detected in WT γ S following exposure to GuHCl for 16 min (Figure 4a). The region of the mass spectrum from $m/z = 906\text{--}918$ contains the +23 charge state of the

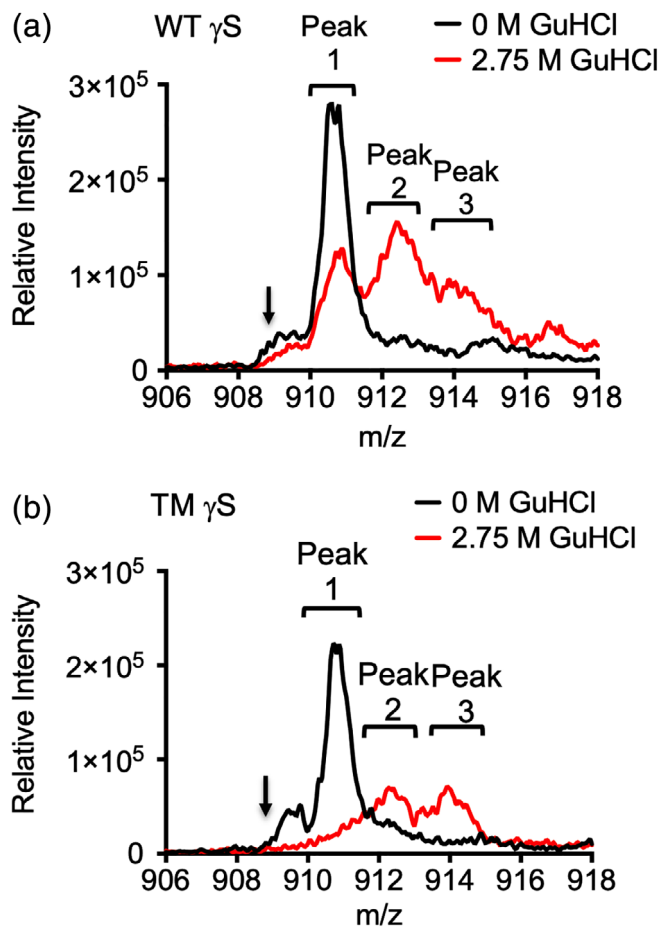


FIGURE 4 Mass spectra of WT and TM γ S during chemical unfolding. Mass spectra of the +23 charge state of WT and TM γ S following partial unfolding in 2.75 M GuHCl. Three major peaks were detected after 16 min in GuHCl with mass increases of 36–43 Da (peak 1), 83–85 Da (peak 2), and 120–130 Da (peak 3) over the peak of the unlabeled proteins at the position of the arrow (spectra not shown). (a) The spectrum of WT γ S incubated in the absence of GuHCl is overlaid with that incubated in GuHCl for 16 min. (b) The spectrum of TM γ S incubated in the absence of GuHCl is overlaid with that incubated in GuHCl for 16 min. In both panels a and c, there is a decrease in Peak 1 (folded species) and an increase in Peak 2 (partially unfolded intermediate) and Peak 3 (nearly fully unfolded species). Spectra are averaged from three independent experiments

protein showing mass increases of \sim 43 Da (Peak 1), \sim 85 Da (Peak 2), and \sim 130 Da (Peak 3) in the GuHCl-treated γ S, compared with the m/z of the unlabeled protein at 908.6 (arrows) (spectrum not shown). Peak 1, the major species observed in samples incubated without GuHCl, results from labeling the most solvent-exposed amides in native γ S. In the spectra of TM (Figure 4b), after 16 min of GuHCl exposure, Peak 1 was completely lost, and only Peaks 2 and 3 were observed, indicating that TM unfolds more rapidly than WT γ S, forming the partially unfolded intermediate in Peak 2, and the nearly

fully unfolded form in Peak 3 at faster rates. Since the exchange was performed in 90% D₂O, and back exchange was estimated to be approximately 10%, Peaks 1, 2, and 3, corresponded to the exchange of approximately 31, 62, and 94% of the protein's backbone amides, respectively. The small peak to the right of the arrows in Figure 4, indicating the position of the +23 ion of the unlabeled proteins, may result from aggregated γ S that is largely unavailable for HDX.

The percentage of Peak 1 (native structure), Peak 2 (partially unfolded intermediate), and Peak 3 (nearly fully unfolded protein) was calculated and the time course of their appearance and decrease after 0–32 min of exposure to 2.75 M GuHCl is shown in Figure 5. At 4, 8, and 16 min, there was a significant decrease in Peak 1 (native structure) in N76D and TM γ S compared with the WT γ S (Figure 5a). The more rapid loss of native structure (Peak 1) in N76D and TM γ S was accompanied by the significantly greater abundance of partially unfolded Peak 2 at 2, 4, and 8 min compared with WT γ S (Figure 5b), and a significantly lower abundance of Peak 2 at 32 min due to the faster accumulation of Peak 3 at 16 and 32 min (Figure 5c). In comparison, N14D and N143D γ S unfolded at similar rates as the WT γ S following GuHCl addition (Figure 5d–f). While the identities of the exchanged amide residues in these three peaks were not determined, these results suggested that deamidation in N76D and TM γ S led to more rapid production of partially and fully unfolded forms when γ S was exposed to GuHCl.

In the absence of denaturant, both WT and deamidated γ S-crystallins showed remarkably slow deuterium uptake reaching only about 45% of their exchangeable amides exchanged after 4 hr of incubation (not considering back exchange) (Figure S3). Limited exchange was similarly observed in earlier HDX experiments with the related β -crystallins,⁴⁴ reflecting the compact folding of their Greek Key motifs. Comparing mass spectra for WT and deamidated γ S, there were not significant differences in the observed HDX (Figure S3A). Indeed, amide hydrogens in TM were slightly less accessible than in WT γ S, incorporating an average of 7.3 Da less at each time point. The raw mass spectra are shown in Figure S3B for WT and TM γ S. While deamidation did not significantly alter the global HDX of γ S as monitored by mass spectrometry, deamidation did lead to more rapid formation of unfolded intermediates during chemical denaturation.

2.4 | Chemically-induced aggregation of wild type and deamidated γ S

To investigate whether surface deamidations of γ S led to the formation of aggregation-prone, partially unfolded

protein states, aggregation of WT and deamidated γ S was monitored under conditions that facilitated unfolding (Figure 6). Proteins were incubated at 37°C in the presence of 2 M GuHCl, that is, a denaturant concentration corresponding to the beginning of the unfolding transition determined in Figure S2. For WT, there was a sigmoidal increase in solution turbidity and thioflavin T (ThT) fluorescence over time which together indicated that the protein was forming aggregates with a degree of ordered fibrillar structure, as reported previously for γ D-crystallin under comparable conditions.⁴⁵ For N14D and N143D, there was a minor but significant ($p < .05$) increase in aggregation propensity relative to WT, as shown by higher rates of aggregation (Figure 6a, inset) as well as higher levels of turbidity and ThT binding at the end of the incubation period (Figure 6b). In contrast, N76D showed a considerably greater aggregation propensity, consistent with its reduced stability (Figure S2) and

faster rate of unfolding under denaturing conditions (Figure 5). The effects of deamidation at each site were cumulative with TM exhibiting the highest propensity to aggregate on the basis of aggregation rate. Despite the higher aggregation rate and final ThT binding, the solution turbidity of TM was disproportionately low, indicating a shift to more elongated (i.e., rod-like) structures.⁴⁶ It is concluded that surface deamidations of γ S, particularly at N76, promotes partial unfolding which thereby leads to enhanced aggregation.

2.5 | Thermally-induced aggregation of wild type and deamidated γ S

The enhanced aggregation propensity of deamidated γ S was further investigated under thermal stress (Figure 7). Turbidity assays were performed in the

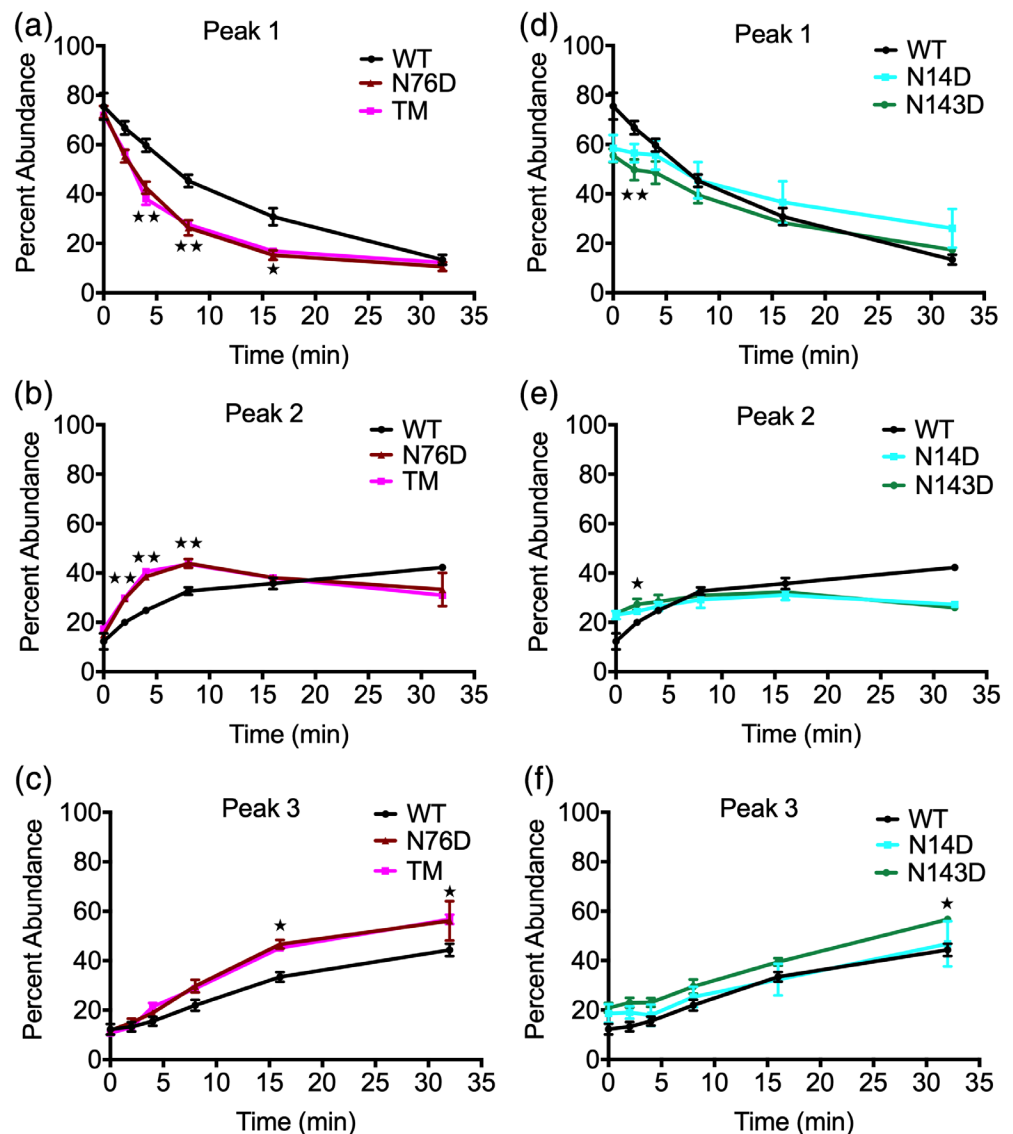


FIGURE 5 Relative abundance of γ S intermediates during chemical unfolding. Percentage under the peak for each species of γ S as shown in Figure 5, calculated using raw mass spectra from pulse labeled protein in D₂O containing buffer. Relative abundance of peaks 1, 2, and 3 for (a–c) N76D and TM compared with WT, and (d–f) N14D and N143D compared with WT. Significant differences from WT γ S determined using Student's *t*-test, *p*-values $\leq .01$ and $\leq .05$ are denoted by ** and *, respectively ($n = 3$)

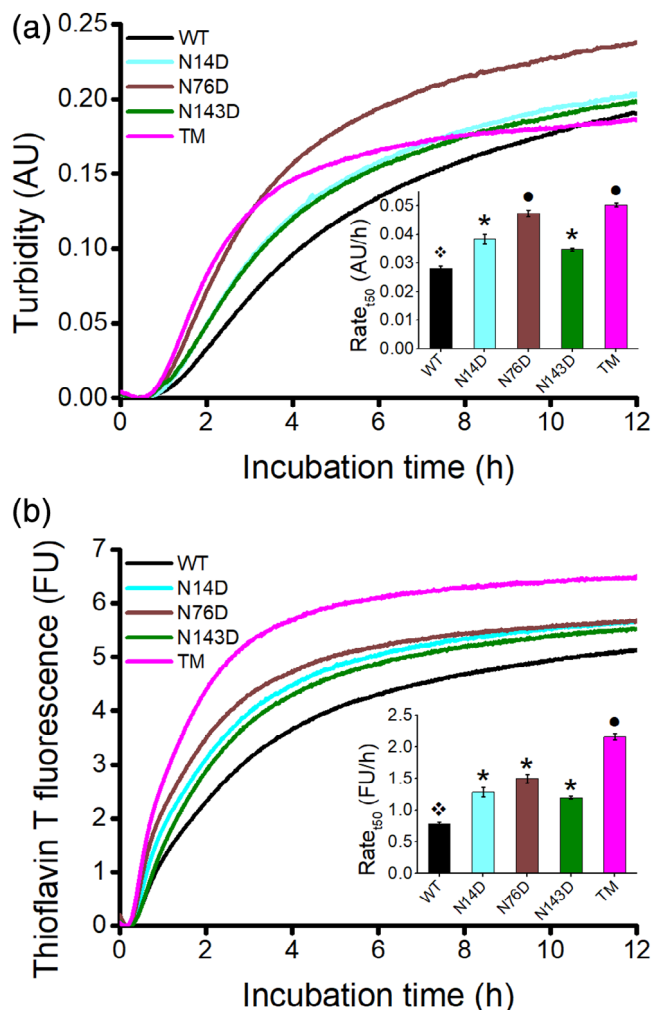


FIGURE 6 Time-course of aggregation of γ S and its deamidation mimics monitored by turbidity and ThT binding. WT and deamidated γ S at 5 mg/ml and in 2.0 M GuHCl were incubated at 37°C. (a) Changes in turbidity at 405 nm. (b) Changes in thioflavin T fluorescence at 440/485 nm. AU and FU represent absorbance and fluorescence units, respectively. Aggregation curves shown are average measurements ($n \geq 2$) representative of three independent experiments. Insets show maximum aggregation rate (Rate_{150}) derived from absorbance and fluorescence curves fitted with Boltzmann and Hill sigmoidal functions, respectively ($n \geq 4$, error bars = SEM). Symbols (i.e., ❖, *, and ●) denote groups of rate_{150} values that are significantly different from each other (p -value $\leq .05$)

presence of oxidized glutathione, GSSG, which reacts with free cysteine sulfhydryl groups (Figure 7a). Samples were buffer exchanged into a NaPi buffer containing 1 mM DTT and then 6 mM GSSG was added before thermal denaturation. The addition of GSSG lowers the temperature for the initiation of aggregation.³⁷ When incubated at 60°C, the TM underwent more rapid aggregation than the WT γ S, similar to that for N14D and N76D.³⁷ There was also increased

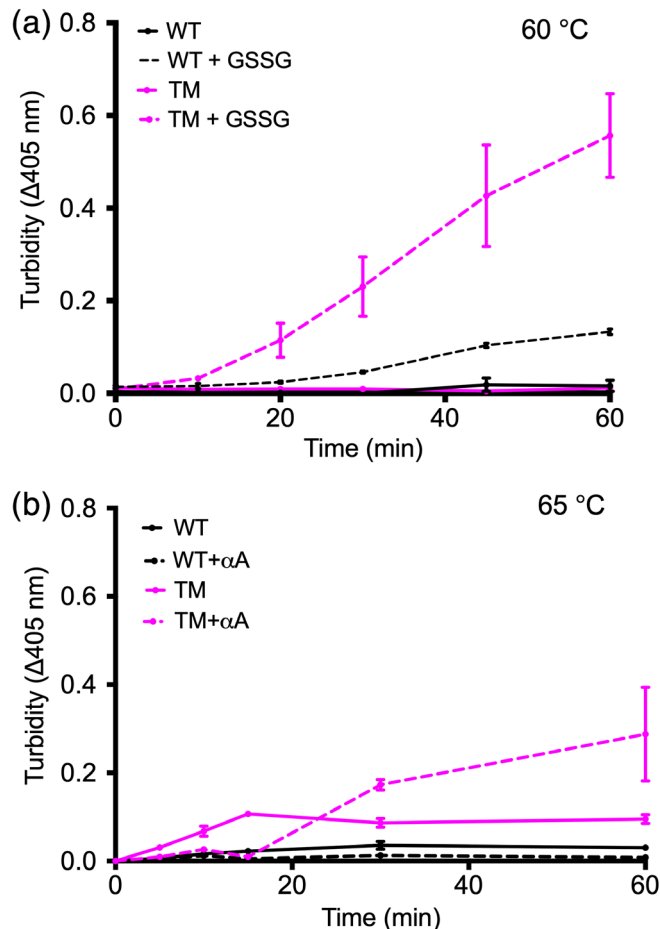


FIGURE 7 Effect of deamidation on thermal-induced aggregation of WT and TM γ S monitored by turbidity and its modulation by either oxidation or the molecular chaperone α A-crystallin (α A). (a). Changes in turbidity during thermal-induced denaturation of WT and TM γ S in the presence of 6 mM GSSG and at 60°C ($n = 3$, error bars = SEM). (b) Changes in turbidity during thermal-induced denaturation of WT and TM γ S in the presence and absence of α A. WT and TM γ S incubated at 65°C with and without α A at a 2:1 ratio of γ S: α A ($n = 4$, error bars = SEM)

variability in TM as noted by the error bars of TM compared with WT with GSSG reflecting the formation of large aggregates in TM compared with WT.

After 60 min at 60°C, samples were digested with trypsin and analyzed by mass spectrometry. A tryptic peptide with an intermolecular disulfide crosslink between two γ S 20–35 peptides was at three-fold higher intensity in the digest of TM compared with WT (Figures S4, S5). This intermolecular crosslink via C24 was previously identified in disulfide-linked dimers of WT γ S that had enhanced aggregation properties compared with monomeric γ S.³⁹ Taken together, these results imply that deamidation of γ S promotes the formation of intermolecular disulfide linkages that, in turn, facilitates its aggregation.

WT and TM γ S were next incubated at 65°C with and without the presence of a 2:1 mass ratio of the molecular chaperone α A-crystallin (α A) to probe differences in chaperone ability introduced by γ S surface deamidations (Figure 7b). The temperature was optimized to detect differences between TM γ S temperature stability with and without the presence of α A. Both WT γ S alone and WT γ S in the presence of α A exhibited little change in light scattering at 405 nm over the course of the experiment, as did the other singly deamidated mutants (Figure S6). As expected, TM γ S alone increased its turbidity over 15 min of heating due to unfolding and aggregation, after which there was no further change. When incubated in the presence of α A, no increase in turbidity of TM γ S occurred during the first 15 min, before aggregation commenced. The large error bar of the TM γ S plus α A sample at 60 min in Figure 7b reflects the variability from the sample precipitating and forming large, light-scattering aggregates. Samples were analyzed by SDS-PAGE and bands from the precipitated protein samples of TM alone and TM with α A were confirmed by mass spectrometry to contain γ S and γ S plus α A, which co-migrate together via SDS-PAGE due to their similar mass (Figure S6 inset). Thus, α A forms an unstable complex with deamidated γ S under thermal stress that ultimately leads to rapid co-aggregation and precipitation. Surface deamidations increased thermally-induced aggregation of γ S that was modulated both by oxidation and by the molecular chaperone, α A.

2.6 | Molecular dynamics simulations of wild type and deamidated γ S

WT and deamidated γ S molecular dynamics (MD) simulations over 125 ns were performed (Figure 8). The data suggest that while WT and N143D had one predominant conformation during the simulation, both N14D and N76D had additional conformations populated during the simulation (Figure 8a). The N76D mutant steadily deviated from its original conformation, while N14D deviated only slightly and WT/N143D did not show any deviation over the time frame (Figure 8b). The distribution plots suggest increased conformational dynamics of N76D compared with WT γ S, a conclusion that is supported by our recent HDX data as monitored by NMR spectroscopy.³⁷ Additionally, MD simulations imply that deamidation at N76 in γ S could result in a nonnative, surface salt bridge between the introduced anionic carboxylate of D76 and the cationic guanidinium group of R78, as shown in Figure 8c.

2.7 | Identification of internal disulfide crosslinks

Three cysteines, C22, C24, and C26, form part of a distinctive sequence, 21-DCDCDC-26, that has been proposed to act as a redox center and involve the formation of at least one intramolecular disulfide bond,^{47,48} most likely between C22 and C26, as occurs in the γ S disulfide-linked dimer.³⁹ In view of a recent report indicating disulfide interchange at this site,⁴⁹ we investigated whether increased dynamics in this region, based on our recent NMR data,³⁷ would disrupt the disulfide arrangement. After buffer exchange to lower reducing agent and incubation under native conditions for 60 min at 37°C, mass peaks of the γ S 20–35 tryptic peptide containing an internal disulfide crosslink and one alkylation were 3–4 times higher in WT than in TM (arrows in Figure 9a,b, respectively). Two peaks in the chromatogram for this peptide were observed, likely due to differences in the position of the disulfide bond between the three cysteines. Assignment of these peak identities requires further analysis of γ S under different redox conditions and examination of possible y10, 11, 12, and 13 fragment ions in the different species to localize disulfide bonds possibly involving C24. The y ion series in this peptide dominate and result from fragmentation of peptide bonds yielding progressively larger ion series from the peptide C-terminus for WT and TM (Figure 9c,d, respectively). A disulfide bond between C22 and C26 would prevent assignment of y10–13 ions, while y10–11 or y12–13 ions would be expected, if disulfide bonds occurred between C22–C24 and C24–C26, respectively. However, based on their close distance from each other in the NMR solution structure of the monomer and observed formation in the crystal structure of the oxidized WT γ S dimer,³⁹ it is predicted that the major internal disulfide is between C22 and C26, which is less prevalent in the triply deamidated protein (Figure 9e).

3 | DISCUSSION

The long-lived crystallin proteins are extensively modified during aging and cataract formation. However, an emerging theme is that many of these age-related modifications do not alter the overall structure or stability of crystallins significantly. Here, we demonstrate that one of the most prevalent modifications, deamidation of surface Asn residues, while causing minimal structural disruption, leads to increased aggregation that could contribute to lens opacification. Deamidation of γ S at the labile N14, N76, and N143 is observed to increase the propensity of the protein to aggregate under physiologically relevant

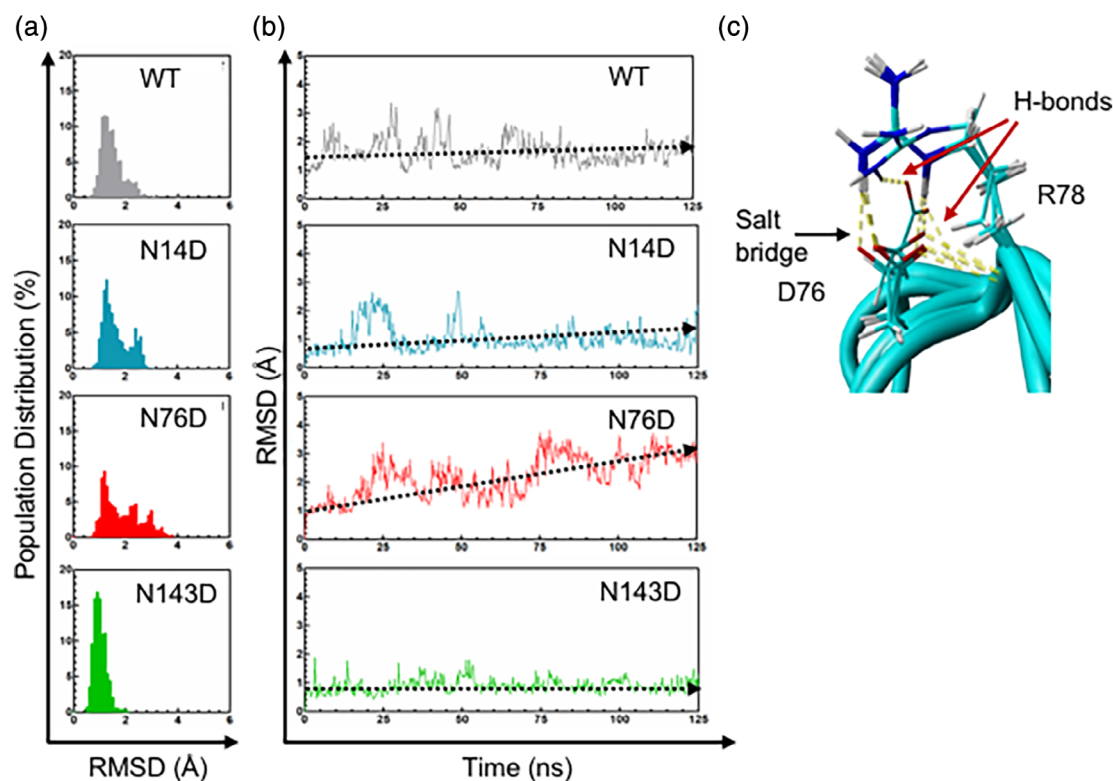


FIGURE 8 Molecular dynamics simulations of γ S. (a) The population distribution of conformations of WT (gray), N14D (teal), N76D (dark red), and N143D (green) γ S. (b) The root-mean-square-deviation (RMSD) in the structural distances during simulation. The solid black lines represent the general trend of the RMSD in the structure. (c) Molecular dynamics simulations showing a potential salt bridge between D76 and R78 (black arrow). Hydrogen bonds are also shown (red arrows)

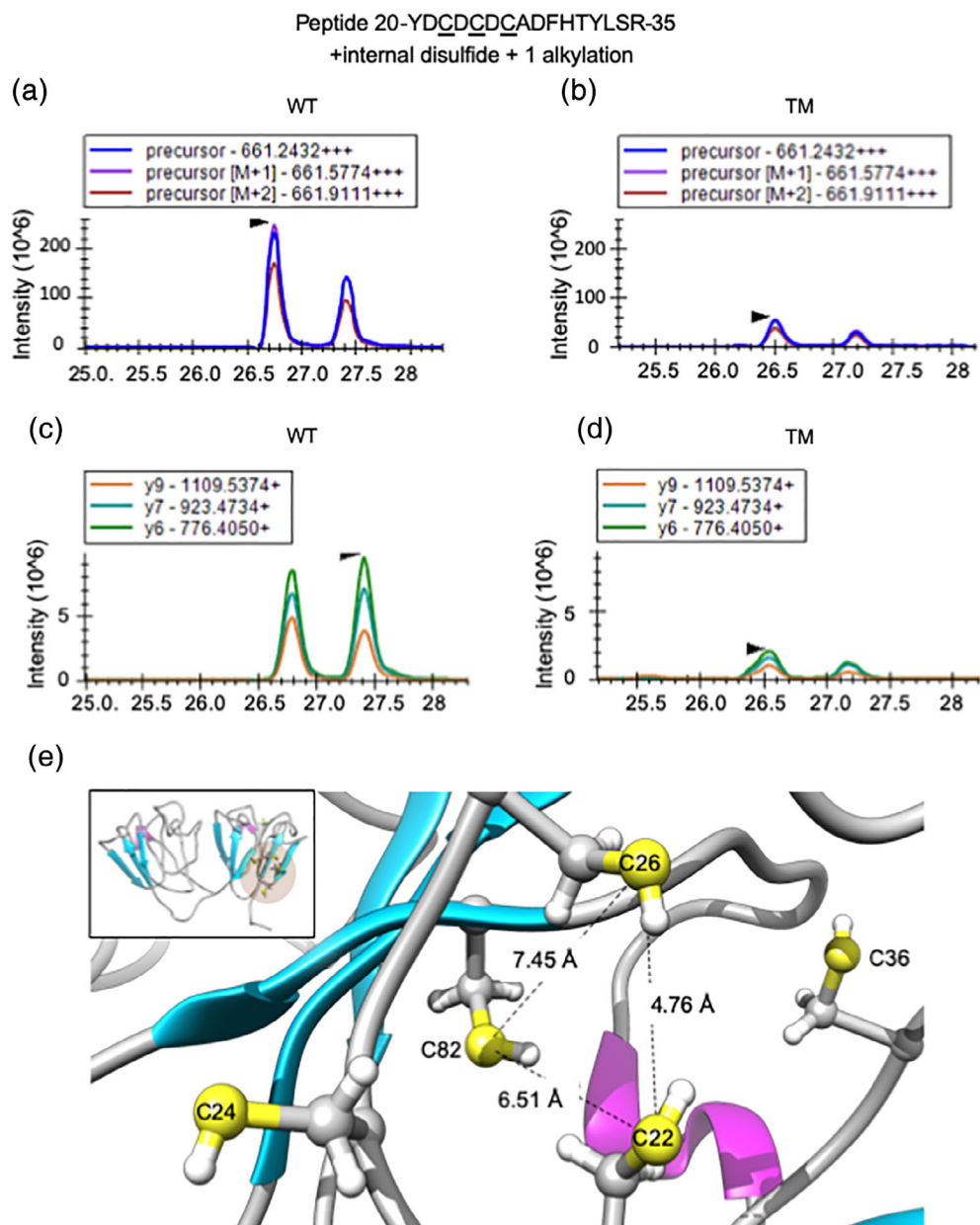
conditions. Importantly, the high intensity of scattered light relative to the protein concentration in solution suggests that a small population (less than 1%) of the protein gives rise to very large aggregates (R_h greater than 10 nm). In systems where proteins are present at concentrations near their saturation limits, proteins are at a significantly higher risk of undergoing aberrant aggregation in response to destabilizing mutations and post-translational modifications.⁵⁰ The eye lens is a highly crowded environment containing $\sim 90\%$ crystallin proteins at 300–400 mg/ml. Thus, while we found less than 1% of γ S-crystallin aggregating under dilute conditions, we expect a higher proportion of modified protein to aggregate in the crowded environment of the lens.

The enhanced aggregation propensity of deamidated γ S was accompanied by only a minor loss of thermodynamic stability, consistent with previous studies on β/γ -crystallins.^{7,38,51} Such results are expected because the high stability of β/γ -crystallins is mainly due to the energetically favorable burial of hydrophobic amino acid residues upon folding.^{42,43} Complementary to this, the surface of β/γ -crystallins is dominated by hydrophilic and charged residues, particularly in loop regions, that form favorable hydrogen bonds with

water, thereby providing solubility and stability.³⁰ Thus, deamidation of surface residues produces less pronounced changes in thermodynamics and solvent accessibility, but nonetheless results, as recent studies have reported, in increases in the association properties of β/γ -crystallins. Specifically, deamidation of β A3 at multiple surface residues leads to higher ordered oligomers,²⁶ dual deamidation of human γ S at N76 and N143 results in greater intermolecular interactions,⁷ and deamidation at N76 leads to a greater tendency toward dimer formation,³⁸ all without significantly perturbing the structure or stability of the protein. Likewise, several γ -crystallin variants associated with congenital and juvenile cataract exhibit little to no difference in their overall structure compared with their respective wild type proteins.^{4,5,8,9,52–54}

Molecular dynamics simulations presented here suggest increase conformational dynamics of N76D compared with WT γ S, consistent with our recent NMR HDX data.³⁷ We propose that deamidation of N76 drives changes in conformational dynamics that lead to increased aggregation. Alteration in dynamics was detected by differences in HDX for backbone NH protons throughout the protein, that is, at sites distant from

FIGURE 9 Mass spectra of a potential disulfide bond in peptide 20–35 of WT and TM γ S. (a and b) Extracted ion chromatograms of the precursor, $M + 1$, and $M + 2$ peaks for the γ S peptide 20–35 containing one internal disulfide bond and one alkylation in its cysteines 22, 24, and 26 for WT and TM γ S, respectively. (c and d) The tracings for the coincident y_6 , 7, and 9 fragment ions for the peptide generated during the parallel reaction monitoring scans during the LC/MS run for WT and TM γ S, respectively. (e) Distances between the proximal C22, C26, and C82 in the solution monomer as generated with <http://www.rbvi.ucsf.edu/chimera/>. (PDB 2M3T)



the mutations including the α -helical regions in both the N- and C-tds.³⁷ Noted changes are in β -strands in the first Greek Key motif near deamidation sites at N14 and N76. Increased exchange suggests enhanced solvent accessibility with a time frame of minutes to days of motion. Thus, deamidated γ S appears to undergo greater conformational fluctuations that expose otherwise slow-exchanging core residues to water, facilitating intermolecular association.^{37,55} MD simulations also suggest the potential for salt bridge formation between the side chains of D76 and R78 that could account for the greater deviation of the conformation of N76D compared with WT γ S. The minor increase in enthalpy accompanying salt bridge formation may come at a cost of

conformational entropy in the vicinity of this region.^{56,57}

Indeed, NMR relaxation measurements indicate there is reduced flexibility in the loop between α -helix a2 and β -strand c2 in N76D compared with the same region in WT γ S (see Figure 8 in reference 37).

The greater exposure of core residues and accessibility of other residues over time predicted from NMR and MD experiments may also account for the increased tendency of deamidated γ S to aggregate under partially denaturing conditions. During chemical kinetic unfolding of γ S, HDX observed a partially unfolded intermediate and a nearly fully unfolded intermediate being formed more rapidly by N76D and TM than WT γ S. At a slightly lower concentration of chemical denaturant, all deamidation

mimics aggregate more rapidly, especially N76D and TM, suggesting that the partially unfolded intermediates are precursors to aggregation. The specific backbone amides undergoing rapid exchange, that is, the regions of the protein exposed in these aggregation-prone, partially unfolded intermediates, have not yet been assigned. Based on the ~40-Da increase in mass detected by HDX, these intermediates likely stem from unfolding of the first Greek Key motif in the N-td. In support of this, the N-td unfolds prior to the more stable C-td and initiates aggregation under denaturing conditions.^{28,42,43,45}

Deamidation in the N-td at N14 and N76 impact the stability, unfolding and aggregation of γ S more than deamidation in the C-td at N143. These site-specific differences reflect, in part, difference in the stability between the N-td and the C-td. Illustrating this is the observation that at least seven separate mutations in the N-td of γ S are associated with early-onset cataract, whereas no inheritable mutations have so far been identified in the C-td of γ S.⁵⁸ The implications for the aging lens is that the C-td can potentially better tolerate modifications without undergoing structural perturbation.

Overall, TM γ S shows the highest degree of perturbation compared with the singularly deamidated mutants, including N76D, implying that γ S is progressively destabilized by successive surface deamidations, with each modification contributing a minor effect. The high stability and solubility of crystallin proteins ensure that the lens is able to remain transparent for decades despite deamidation and a myriad of other post-translational modifications, such as truncation and oxidation, occurring over the life of the organism.¹¹ Deamidated crystallins are more susceptible to digestion²⁵ as well as oxidation-induced aggregation.³⁷ Our data suggest that crystallins accumulate age-related modifications to such an extent that large-scale destabilization occurs, leading to their aggregation, insolubilization, and ultimately cataract (as outlined schematically in Figure 10).

The degree of deamidation-induced aggregation of γ S under conditions of partial unfolding depends on the location of the deamidation site (Figure 6 and reference 37). Deamidation and oxidation (in the presence of GSSG), as occurs in the aging lens, together enhance the aggregation of γ S. There are seven cysteine residues in γ S of which four are buried with low solvent-accessible surface area (1–2%) and three have high accessibility, particularly C24 (21–77%).^{36,39} Of the buried cysteine residues, C36, C82, and C114 become more accessible in the deamidated mimics, while one of the accessible cysteine residues, C26, becomes less accessible.³⁷ In the solution structure of γ S, C82 is in close proximity to C22 and C26 (Figure 9e) which are, in turn, proximal to the solvent-exposed C24. Together, these four residues have been

proposed to form a cysteine tetrad that shuffles intramolecular disulfides to maintain γ S in a soluble, monomeric form.⁴⁹ Our findings suggest that deamidation-increased dynamics of γ S disrupt such intramolecular disulfides and thereby increase the susceptibility of γ S to non-native intermolecular crosslinks, such as those observed between C24 residues.^{39,59} Future studies are needed to determine if other cysteine residues are modified and are therefore associated with the aggregation of the different deamidated γ S-crystallins.

Finally, there is growing evidence to suggest that the molecular chaperone action of α -crystallin, the first line of defense against protein misfolding and aggregation in the lens, becomes impaired as crystallins are progressively deamidated. Thus, α A is relatively ineffective at chaperoning TM γ S under temperature stress with the interaction of both proteins leading to co-aggregation and co-precipitation. Several reports support these findings and indicate that α -crystallins are less efficient at chaperoning more rapidly aggregating proteins, including deamidated crystallins.^{24,38,60–63} Adding to this, deamidation of α A directly can lead to a partial loss of its chaperone ability.⁶⁴ Thus, it is evident that deamidation disrupts lens protein homeostasis (proteostasis) via several mechanisms. Once deamidation accumulates in the lens beyond a critical threshold, a cascade of nucleation-dependent crystallin aggregation and subsequent precipitation is initiated.⁶⁵ This may apply also to other age-related, protein aggregation diseases such as Alzheimer's in which deamidation of long-lived proteins has been implicated in amyloid fibril aggregation.^{11,66}

4 | CONCLUSION

Lens crystallins undergo extensive deamidation during aging and cataract formation. We have mimicked the aging process in crystallins by introducing deamidations via mutation in γ S. Our recently published findings and those presented here support a model in which the formation and/or maintenance of an intramolecular disulfide crosslink is disrupted by increased conformational dynamics due to deamidation (Step 1 in Figure 10). The deamidated monomer favors a “disulfide-unlocked” state (Figure 10, blue arrow between the two Greek Key motifs in the N-terminal domain) that further increases oxidation at susceptible surface cysteines such as C24 (Step 2 in Figure 10), leading to more aggregation-prone crosslinked-dimers (Step 3 in Figure 10). Our findings also support that a small amount of the deamidated monomer can form large light scattering aggregates directly without prior heat or oxidation (thin arrow in Figure 10). Such effects are cumulative with more heavily

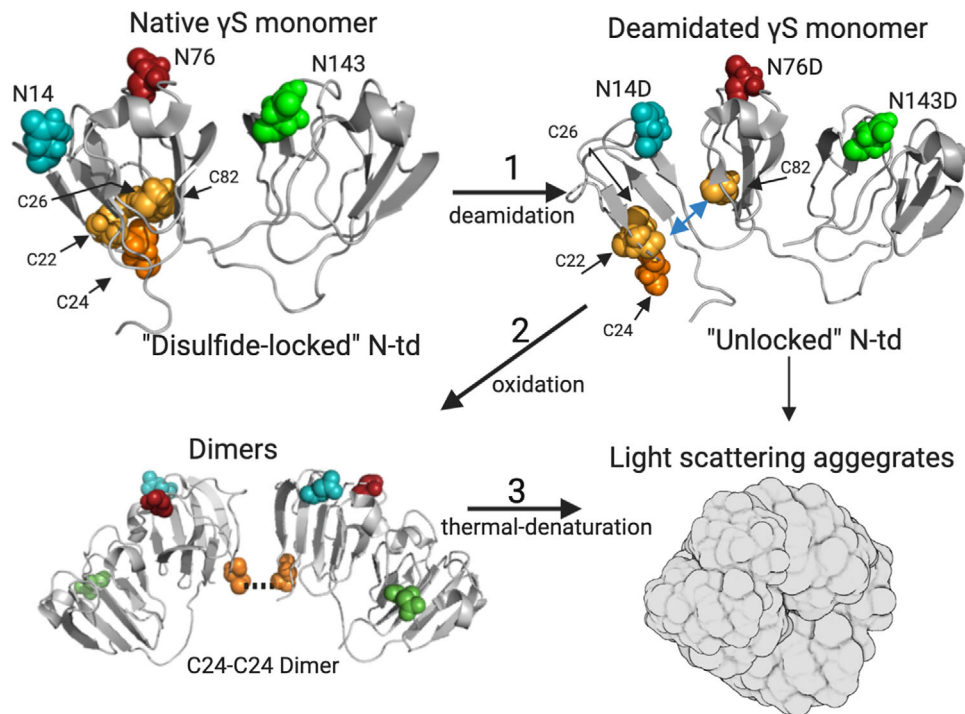


FIGURE 10 Potential γ S aggregation pathways due to cataract-associated deamidations. Our data support a model where native γ S monomer has an internal disulfide bond that “locks” the N-terminal domain (N-td) into a conformation that is “unlocked” by increased conformational dynamics due to deamidation (Step 1). The deamidated monomer favors a “disulfide-unlocked” state (blue arrow between the two Greek Key motifs in the N-td) that is predisposed to oxidation at surface cysteines (Step 2, dotted line), leading to more aggregation-prone crosslinked-dimers (Step 3). A small amount of the deamidated monomer can also form large light scattering aggregates directly (thin arrow). Created with BioRender.com

modified (“aged”) crystallins tending to partially unfold more readily, exposing hydrophobic residues that lead to aggregation and ultimately precipitation, causing the opacification of the eye lens associated with cataract.

5 | MATERIALS AND METHODS

5.1 | Recombinant expression and purification of human γ S and deamidation mimics

The plasmid containing the gene for WT γ S was obtained from the plasmid repository at DNASU (<https://dnasu.org/DNASU/Home.do>). Single deamidation mimics of N14, N76, and N143, along with the triple mimic of all three sites, were generated via site-directed mutagenesis using the QuikChangeXL Kit (Agilent Technologies, CA). Protein was expressed in a pE-SUMO (Small Ubiquitin-like Modifier) vector containing a N-terminal 6XHis tagged fusion protein (LifeSensors Inc., PA) using *Escherichia coli*. Cells were cultured at 37°C, protein expression was induced with IPTG, and growth continued at 37°C for 4 hr. Purification of the protein used HisPur Cobalt Resin

following the manufacturer’s protocol (Thermo Fisher Scientific, Waltham, MA.). The removal of the His Tag and SUMO was performed using Ulp-1 protease (Ubl-specific protease 1). Protein was then run through HisPur Cobalt Resin again to remove the tag. Protein stocks were aliquoted, reduced with 2.4 mM dithiothreitol (DTT), and stored at -80°C . Typical yields of protein were several mg per 100 ml of *E. coli* culture. The purity ($> 95\%$) and masses of all expressed proteins were confirmed by MS and SDS-PAGE. Protein concentrations were determined from the absorbance at 280 nm and using the extinction coefficient of $42,860 \text{ cm}^{-1}/\text{M}$ for human γ S (Expasy ProtParam). Recombinant expression and purification of human α A crystallin was as previously described.²⁴

5.2 | DLS of WT and deamidated γ S

Proteins were concentrated to 1 or 5 mg/ml using centrifugation (Amicon Ultra-15 Filter Units [10 kDa MWCO], Millipore Sigma, Burlington, MA). Samples were exchanged into Buffer A (60 mM NaPi [pH 6.8], 100 mM KCl, 1 mM EDTA and 1 mM DTT) using dialysis and cleared of large particulate matter using 0.1 μm pore size

filters (Ultrafree-MC Centrifugal Filter Units, Millipore Sigma). Samples of 30 μL were loaded into a 384 well plate in replicates of 5 for each protein and the DLS measured at 25°C using a DynaPro Plate Reader III (Wyatt Technology Corporation, Santa Barbara, CA). The primary measurement of time-dependent fluctuations of scattered light was converted to radii of the constituent species in the sample using autocorrelation analysis and the regularization algorithm of DYNAMICS software (Wyatt Technology). The results were plotted as a distribution of radii of constituent species of the sample. Species of comparable radii were binned (Peak 1:1–10 nm; Peak 2:10–100 nm; Peak 3:100–1,000 nm) and the spread of the resulting population is expressed by its polydispersity (%Pd).

5.3 | Size-exclusion chromatography and multi-angle light scattering (SEC-MALS) of WT and deamidated γS

WT and deamidated γS were buffer exchanged and concentrated as described for DLS above. The weight average molecular weights (M_w) were determined from the measured Rayleigh light scattering (DAWN Heleos II and ASTRA 7 Software, Wyatt Technology). Absorbance at 280 nm or determination of the differential refractive index of the solution (using a refractive index increment of 0.193 for γS and refractometer Optilab REX, Wyatt Technology) were used to determine concentration.⁷ Fractions eluting under each peak were analyzed by SDS-PAGE. The eluting fractions containing the monomer peaks for WT and TM γS were next collected, concentrated as above for DLS and incubated for 6 days at 37°C. Samples were then reanalyzed by SEC-MALS to detect aggregates that had formed from the monomers with time. The polydispersity index (PDI) was determined from the ratio of M_w to M_n (i.e., M_w/M_n), where M_n is the number average molecular weight. A monodisperse sample would have a PDI of 1.000. All values were calculated in ASTRA 7 software and variability is a percentage of the average value under the protein peak (Wyatt Technology). The percent of protein eluting in each peak was determined from the amount of protein recovered for that peak compared with the total amount of protein recovered in all the peaks, using the in-line refractive index detector as the concentration source.

The presence of protein eluting in the high molecular peak near the void volume was confirmed by MS. Briefly, samples were reduced and alkylated with dithiothreitol and iodoacetamide respectively. Proteins were digested overnight with trypsin and the resultant peptides were analyzed by LC-MS/MS on a Thermo Orbitrap Fusion Mass Spectrometer with a Thermo UltiMate 3,000 HPLC (Thermo Scientific,

San Jose, CA). Peptides were then identified using a human Uniprot database and Sequest search within the Protein Discoverer Suite (Thermo Scientific), and only peptides with a false discovery rate below 1% were accepted.

5.4 | Equilibrium chemical unfolding of WT and deamidated γS

Proteins were denatured with increasing amounts of GuHCl using methods previously described by Mills et al.,⁴³ for direct comparison (100 mM NaPi [pH 7.0], 1 mM EDTA, and 5 mM DTT) at 37°C overnight with a final protein concentration of 10 $\mu\text{g}/\text{ml}$. Samples were excited at 295 nm and emission spectra measured from 310–400 nm with slit widths set at 0.5 mm using a spectrofluoropolarimeter (Photon Technology Inc., NJ). The ratio of the 360 to 320 nm fluorescence intensities were used to calculate percent protein unfolded at each GuHCl concentration. Nonlinear line fit was performed using KaleidaGraph (Synergy Software, Reading, PA) as previously described from 1 to 3 independent experiments.²⁵ All curves had a correlation coefficient, R , equal to 0.998–0.999 and best fitted to a two-state unfolding curve. The $\Delta G^\circ_{\text{N-U}}$ was determined as previously described using the $\text{RTln}K_{\text{eq}}$ values calculated for $K_{\text{eq}} = f_{\text{U}}/f_{\text{N}}$ from the transition region of the GuHCl denaturation curves.²⁵

5.5 | Global hydrogen-deuterium exchange of WT and deamidated γS

In order to determine the global HDX of γS , continuous labeling of intact WT and deamidated γS was initiated by dilution of 5 μL of protein stock (300 pmol) into 25 μL of HDX buffer (20 mM NaPi [pD 7.4], 1 mM EDTA, 2.5 mM TCEP, and 150 mM NaCl in D_2O) at 25°C. At time points ranging from 10 s to 4 hr, samples were quenched to pH 2.3 in 25 μL of 4 M GuHCl, 200 mM KPi, 0.72 M TCEP and 4°C. Deuterium incorporation was measured by LC/MS on a Xevo G2 QToF mass spectrometer (Waters Corp., Milford, MA). The overall deuterium incorporation of each protein was calculated by deconvoluting the intact mass spectra of the protein and subtracting the weight of the deuterated protein from the undeuterated at each time point. HDX in deamidated γS was compared with that for WT γS . Each time point was replicated five times for WT γS and twice for deamidated γS .

In order to measure the rates of unfolding in GuHCl, proteins were incubated in 2.75 M GuHCl and pulse labeled for 1 min in D_2O buffer. The number of amide hydrogens exchanged with deuterium was determined by measurement of the masses of whole proteins. Samples were diluted

to 0.9 mg/ml in buffer containing 50 mM NaPi (pH 7.4), 300 mM NaCl, 10 mM imidazole, and 10 mM DTE. Diluted protein (10 μ l) was mixed with 40 μ l of 3.44 M GuHCl in H₂O exchange buffer (20 mM NaPi (pH 7.4), 2.5 mM TCEP, and 1 mM EDTA). After unfolding for 0–32 min at 30°C, 10 μ l of each GuHCl-treated sample was mixed with 90 μ l of D₂O exchange buffer for 1 min at 30°C. Labeling was quenched by addition of 25 μ l ice-cold 0.8 M phosphate buffer (pH 2.4) and samples immediately frozen on dry ice. Masses of unexchanged proteins were determined by similar treatment, but by adding 90 μ l of H₂O exchange buffer instead. Mass analysis of γ S was performed by individually and reproducibly thawing each sample and immediate injection onto an ice submerged 1 \times 8 mm Opti-Trap™ protein trap cartridge (Optimized Technologies, Oregon City, OR) at 50 μ l/min in a mobile phase containing 0.1% formic acid and 2% acetonitrile. After washing for 3 min, proteins were eluted in mobile phase containing 0.1% formic acid and 80% acetonitrile and mass measured using a LTQ Velos ion trap mass spectrometer (Thermo Scientific) using MS scans in enhanced mode. Spectra acquired during the \sim 30 s protein elution were averaged, and measurements at each time point repeated three times in independent experiments. The region of the spectra from m/z 906 to 918 containing the +23 ion was used to calculate the number of deuteriums exchanged into the various species at each time during GuHCl unfolding. The area of the three major peaks of deuterated protein were calculated and expressed as the percent of total area of all observed peaks.

5.6 | Chemically-induced aggregation of WT and deamidated γ S

Unfolding and aggregation induced by GuHCl were monitored using a Synergy 2 Microplate Reader (BioTek, Winooski, VT). Proteins were initially concentrated to 10 mg/ml using Ultra-0.5 ml Filter Units (10 kDa MWCO) and filtered with Millex-GV Syringe Filter Units (0.22 μ m pore size). Samples were then prepared at 5 mg/ml in 25 mM NaPi (pH 7.2), 100 mM NaCl, with 10 mM DTT and 2 M GuHCl. Protein samples (60 μ l) were transferred to black μ CLEAR® 96-well microplates (Greiner Bio-One, Monroe, NC; Catalogue No. 675096) which were then sealed with MiniStrips™ (Excel Scientific, Victorville, CA; Catalogue No. SP-2 \times 8–50). Microplates were incubated with continuous shaking (1,140 rpm) at 37°C. Turbidity (405 nm) and ThT fluorescence (excitation/emission at 440 \pm 20/485 \pm 10 nm) were measured every minute for 12 hr.

Aggregation kinetics were fitted to a sigmoidal functions using Origin Pro 9.0 (OriginLab Corporation, Northampton, MA) and the fitting parameters were used

to calculate the maximum rate of aggregation as previously described.⁶³ Turbidity and ThT binding curves were fitted with the single Boltzmann and the modified Hill function, respectively.

5.7 | Thermally-induced aggregation of WT and deamidated γ S

Proteins were heated at 60°C (i.e., below the onset of thermal unfolding³⁹) and changes in turbidity measured. WT and TM γ S at 1 mg/ml in 25 mM NaPi (pH 6.8), 100 mM KCl, 1 mM EDTA and 1 mM DTT were oxidized by addition of 6 mM GSSG and incubation at 60°C for 1 hr. Controls were also included without GSSG addition. Samples were heated in a Peltier Thermal Cycler-200 (MJ Research, CA) and the turbidity of each solution was measured in 96-well plate as the change in absorbance at 405 nm using a Synergy-HT Microplate Reader (BioTek).

5.8 | Identification of the disulfide bonding in GSSG incubated γ S

At the end of the 1 hr incubation, iodoacetamide (IAA) was added at a final 5 mM concentration and samples placed on ice. Then, 25 μ l portions containing approximately 20 μ g protein was fully alkylated by addition of 20 μ l of 0.2% ProteaseMax™ detergent (ProMega), 28 μ l 50 mM ammonium bicarbonate buffer, and 2 μ l of 0.5 M IAA. After 15 min incubation at room temperature in the dark, 25 μ l of 0.1 μ g/ μ l Pierce MS grade trypsin (ThermoFisher Scientific) was added, samples incubated at 37°C for 3 hr with shaking, and 2 μ l of formic acid added. Samples were then centrifuged for 5 min at 16,000 g, and 2 μ l of the supernatant (0.4 μ g of peptide) analyzed by LC/MS. Peptides were trapped using a Symmetry C18 nanoAcquity, 100 Å, 5 μ m, 180 μ m \times 20 mm trap column (Waters, Part No. 186006527) at 5 μ l/min in 98% mobile phase A containing water and 0.1% formic acid, and 2% mobile phase B containing acetonitrile and 0.1% formic acid. At 5 min the trap was placed on-line to a NanoEase M/Z Peptide BEH C18, 1.7 μ m, 75 μ m \times 250 mm column (Waters, Part No. 186008795) flowing at 0.3 μ l/min. Peptides were eluted using a 7.5–30% mobile phase B gradient over 30 min and electrosprayed using a NanoFlex source and stainless steel nanobore emitter (Thermo Scientific Cat. No ES542). Mass spectra were collected using a Q-Exactive HF instrument (Thermo Scientific). Precursor scans were collected at 120,000 resolution with an AGC target of 3E6, 200 ms maximum ion time, and 275–1,500 m/z range, followed by parallel reaction monitoring (PRM) scans. Mass/charge

(*m/z*) values of all cysteine containing peptides in γ S in IAA-alkylated, glutathionylated, and interchain disulfide-linked states, including forms of γ S peptide 20–35 with and without intrachain disulfide crosslinks were calculated. In all, a list of 53 *m/z* values were monitored using 15,000 resolution scans, with an ACG target of 100 ms, isolation window of *m/z* = 2, normalized collision energy of 26, and a loop count of 10 to interject precursor scans after each group of 10 PRM scans. Data analysis was performed using Skyline software⁶⁷ to create ion chromatograms for both precursors and fragment ions. For disulfide-linked peptides, cysteines in individual peptides were modified with the calculated mass of other cysteine containing peptides using their elemental compositions after subtracting two hydrogens due to the disulfide bond. This allowed calculation and generation of ion chromatograms for *y* and *b* ions of each of the two peptides involved in the crosslink. The full Skyline analysis dataset will be available from the Panorama Public Repository upon publication.⁶⁸

5.9 | Thermally-induced aggregation of WT and deamidated γ S in the presence of the molecular chaperone, α A-crystallin

For chaperone assays, either WT or TM γ S were mixed with α A at a concentration of a 2:1 ratio (0.66 and 0.33 mg/ml, respectively). Control samples contained 0.66 mg/ml of either WT or TM γ S. Samples were prepared in triplicate with 100 mM NaPi (pH 6.8), 100 mM KCl, 1 mM EDTA, and 2.5 mM TCEP, and incubated at 65°C. The temperature was optimized to detect differences between TM and TM γ S with α A. To determine the identity of the precipitating species, samples were centrifuged, and the soluble proteins separated from the pellet. The pellet was washed, recentrifuged and the remaining insoluble proteins resolubilized. Both the soluble and insoluble proteins were analyzed by SDS-PAGE. After visualization with Coomassie blue staining, protein bands were excised, digested in-gel with trypsin using the ProteaseMaxTM digestion protocol (ProMega Corporation, Madison, WI) and proteins identified by MS using an Orbitrap Fusion mass spectrometer (Thermo Scientific) and data analysis as described as above.

5.10 | Mutant modeling and molecular dynamics simulations of γ S

The solution structure of γ S (PDB 2M3T) was used for modeling the N76D deamidation and the MD simulations were conducted using YASARA *Structure* modeling software (YASARA Biosciences GmbH, Vienna, Austria).

The AMBER ff14 force field was used for full structure energy minimizations, using an explicit solvent TIP3P water model. Molecular dynamic simulations were run for 125 ns, with snapshots taken every 250 ps, using the YASARA MD run macro with explicit solvent conditions at 298 K with a physiological intracellular NaCl concentration. The RMSD frequency distribution (compared with PDB 2M3T) over the 125 ns simulation was calculated in intervals of 0.1 Å and the RMSD of the structure was plotted as a function of time using GraphPad. Structural depiction of the interaction between D76 and N78 in γ S was carried out using YASARA.

5.11 | Statistical analysis

Data presented are the mean \pm SEM. Statistical differences were analyzed using a *t* test with *p* < .05 or less as indicated in each figure. Data were fitted to either a linear or nonlinear regression line and plotted using KaleidaGraph Software (Synergy, Reading, PA) or Prism 6.0 software (GraphPad, San Diego, CA).

ACKNOWLEDGMENTS

The authors thank Wyatt Technology for use of the DynaPro Plate Reader III and Dr. David Anderson for helping to generate Figure 9e.

CONFLICT OF INTEREST

The authors have no conflict of interests to declare.

AUTHOR CONTRIBUTIONS

Calvin Vetter: Formal analysis; investigation; writing-review and editing. **David Thorn:** Formal analysis; investigation; validation; writing-review and editing. **Samuel Wheeler:** Investigation; visualization. **Charlie Munderff:** Investigation; methodology. **Kate Halverson:** Investigation. **Thomas Wales:** Methodology. **John Engen:** Methodology. **Ujwal Shinde:** Formal analysis; investigation; visualization. **Larry David:** Funding acquisition; investigation; methodology; writing-review and editing. **John Carver:** Funding acquisition; project administration; resources; writing-original draft; writing-review and editing. **Kirsten Lampi:** Conceptualization; funding acquisition; project administration; resources; supervision; writing-original draft; writing-review and editing.

ORCID

Kirsten J. Lampi  <https://orcid.org/0000-0002-7906-6699>

REFERENCES

1. Delaye M, Tardieu A. Short-range order of crystallin proteins accounts for eye lens transparency. *Nature*. 1983;302:415–417.

2. Truscott RJ, Friedrich MG. The etiology of human age-related cataract. Proteins don't last forever. *Biochim Biophys Acta*. 2016;1860:192–198.
3. Congdon N, Vingerling JR, Klein BE, et al. Prevalence of cataract and pseudophakia/aphakia among adults in the United States. *Arch Ophthalmol*. 2004;122:487–494.
4. Ji F, Jung J, Gronenborn AM. Structural and biochemical characterization of the childhood cataract-associated R76S mutant of human γ D-crystallin. *Biochemistry*. 2012;51:2588–2596.
5. Ji F, Jung J, Koharudin LM, Gronenborn AM. The human W42R gammaD-crystallin mutant structure provides a link between congenital and age-related cataracts. *J Biol Chem*. 2013;288:99–109.
6. Wilmarth PA, Tanner S, Dasari S, et al. Age-related changes in human crystallins determined from comparative analysis of post-translational modifications in young and aged lens: Does deamidation contribute to crystallin insolubility? *J Proteome Res*. 2006;5:2554–2566.
7. Pande A, Mokhor N, Pande J. Deamidation of human gammaS-crystallin increases attractive protein interactions: Implications for cataract. *Biochemistry*. 2015;54:4890–4899.
8. Boatz JC, Whitley MJ, Li M, Gronenborn AM, van der Wel PCA. Cataract-associated P23T γ D-crystallin retains a native-like fold in amorphous-looking aggregates formed at physiological pH. *Nat Commun*. 2017;8:15137–15137.
9. Ji F, Koharudin LM, Jung J, Gronenborn AM. Crystal structure of the cataract-causing P23T gammaD-crystallin mutant. *Proteins*. 2013;81:1493–1498.
10. Treweek TM, Meehan S, Ecroyd H, Carver JA. Small heat-shock proteins: Important players in regulating cellular proteostasis. *Cell Mol Life Sci*. 2015;72:429–451.
11. Carver JA, Ecroyd H, Truscott RJW, Thorn DC, Holt C. Proteostasis and the regulation of intra- and extracellular protein aggregation by ATP-independent molecular chaperones: Lens α -crystallins and milk caseins. *Acc Chem Res*. 2018;51:745–752.
12. Brubaker WD, Martin RW. (1)H, (1)(3)C, and (1)(5)N assignments of wild-type human gammaS-crystallin and its cataract-related variant gammaS-G18V. *Biomol NMR Assign*. 2012;6: 63–67.
13. Basak A, Bateman O, Slingsby C, et al. High-resolution X-ray crystal structures of human gammaD crystallin (1.25 Å) and the R58H mutant (1.15 Å) associated with aculeiform cataract. *J Mol Biol*. 2003;328:1137–1147.
14. Bax B, Lapatto R, Nalini V, et al. X-ray analysis of beta B2-crystallin and evolution of oligomeric lens proteins. *Nature*. 1990;347:776–780.
15. Van Montfort RL, Bateman OA, Lubsen NH, Slingsby C. Crystal structure of truncated human betaB1-crystallin. *Protein Sci*. 2003;12:2606–2612.
16. Lampi KJ, Murray MR, Peterson MP, et al. Differences in solution dynamics between lens beta-crystallin homodimers and heterodimers probed by hydrogen-deuterium exchange and deamidation. *Biochim Biophys Acta*. 2016;1860: 304–314.
17. Lampi KJ, Ma Z, Shih M, et al. Sequence analysis of betaA3, betaB3, and betaA4 crystallins completes the identification of the major proteins in young human lens. *J Biol Chem*. 1997; 272:2268–2275.
18. Robinson NE, Lampi KJ, Speir JP, Kruppa G, Easterling M, Robinson AB. Quantitative measurement of young human eye lens crystallins by direct injection Fourier transform ion cyclotron resonance mass spectrometry. *Mol Vis*. 2006;12:704–711.
19. Lampi KJ, Ma Z, Hanson SR, et al. Age-related changes in human lens crystallins identified by two-dimensional electrophoresis and mass spectrometry. *Exp Eye Res*. 1998;67:31–43.
20. Dasari S, Wilmarth PA, Reddy AP, Robertson LJ, Nagalla SR, David LL. Quantification of isotopically overlapping deamidated and 18O-labeled peptides using isotopic envelope mixture modeling. *J Proteome Res*. 2009;8:1263–1270.
21. Hooi MY, Raftery MJ, Truscott RJ. Racemization of two proteins over our lifespan: Deamidation of asparagine 76 in gammaS crystallin is greater in cataract than in normal lenses across the age range. *Invest Ophthalmol Vis Sci*. 2012;53:3554–3561.
22. Flaugh SL, Mills IA, King J. Glutamine deamidation destabilizes human gammaD-crystallin and lowers the kinetic barrier to unfolding. *J Biol Chem*. 2006;281:30782–30793.
23. Lampi KJ, Amyx KK, Ahmann P, Steel EA. Deamidation in human lens betaB2-crystallin destabilizes the dimer. *Biochemistry*. 2006;45:3146–3153.
24. Lampi KJ, Kim YH, Bachinger HP, et al. Decreased heat stability and increased chaperone requirement of modified human betaB1-crystallins. *Mol Vis*. 2002;8:359–366.
25. Takata T, Oxford JT, Brandon TR, Lampi KJ. Deamidation alters the structure and decreases the stability of human lens betaA3-crystallin. *Biochemistry*. 2007;46:8861–8871.
26. Takata T, Oxford JT, Demeler B, Lampi KJ. Deamidation destabilizes and triggers aggregation of a lens protein, betaA3-crystallin. *Protein Sci*. 2008;17:1565–1575.
27. Wilmarth P, David L, Lampi K. Normal age-related changes: Crystallin modifications, lens hardening. In: Dartt DA, Besharse JC, Dana R, editors. *Encyclopedia of the eye*. Italy: Academic Press, 2010; p. 161.
28. Kim YH, Kapfer DM, Boekhorst J, et al. Deamidation, but not truncation, decreases the urea stability of a lens structural protein, betaB1-crystallin. *Biochemistry*. 2002;41:14076–14084.
29. Takemoto L, Boyle D. Increased deamidation of asparagine during human senile cataractogenesis. *Mol Vis*. 2000;6: 164–168.
30. Lapko VN, Purkiss AG, Smith DL, Smith JB. Deamidation in human gamma S-crystallin from cataractous lenses is influenced by surface exposure. *Biochemistry*. 2002;41: 8638–8648.
31. Fujii N, Takata T, Fujii N, Aki K. Isomerization of aspartyl residues in crystallins and its influence upon cataract. *Biochim Biophys Acta*. 2016;1860:183–191.
32. Hooi MY, Raftery MJ, Truscott RJ. Age-dependent deamidation of glutamine residues in human gammaS crystallin: Deamidation and unstructured regions. *Protein Sci*. 2012;21: 1074–1079.
33. Hanson SR, Hasan A, Smith DL, Smith JB. The major in vivo modifications of the human water-insoluble lens crystallins are disulfide bonds, deamidation, methionine oxidation and backbone cleavage. *Exp Eye Res*. 2000;71:195–207.
34. Hains PG, Truscott RJ. Post-translational modifications in the nuclear region of young, aged, and cataract human lenses. *J Proteome Res*. 2007;6:3935–3943.

35. Fraczekiewicz RB, Braun W. Exact and efficient analytical calculation of the accessible surface areas and their gradients for macromolecules. *J Comput Chem.* 1998;19:319–333.
36. Roskamp KW, Kozlyuk N, Sengupta S, Bierma JC, Martin RW. Divalent cations and the divergence of betagamma-crystallin function. *Biochemistry.* 2019;58:4505–4518.
37. Forsythe HM, Vetter CJ, Jara KA, et al. Altered protein dynamics and increased aggregation of human γ S-crystallin due to cataract-associated deamidations. *Biochemistry.* 2019;58:4112–4124.
38. Ray NJ, Hall D, Carver JA. Deamidation of N76 in human gammaS-crystallin promotes dimer formation. *Biochim Biophys Acta.* 2016;1860:315–324.
39. Thorn DC, Grosas AB, Mabbitt PD, Ray NJ, Jackson CJ, Carver JA. The structure and stability of the disulfide-linked γ S-crystallin dimer provide insight into oxidation products associated with lens cataract formation. *J Mol Biol.* 2019;431:483–497.
40. Jiang J, Golchert KJ, Kingsley CN, Brubaker WD, Martin RW, Mukamel S. Exploring the aggregation propensity of γ S-crystallin protein variants using two-dimensional spectroscopic tools. *J Phys Chem B.* 2013;117:14294–14301.
41. Serebryany E, Takata T, Erickson E, Schafheimer N, Wang Y, King JA. Aggregation of Trp>Glu point mutants of human gamma-D crystallin provides a model for hereditary or UV-induced cataract. *Protein Sci.* 2016;25:1115–1128.
42. Mills-Henry IA, Thol SL, Kosinski-Collins MS, Serebryany E, King JA. Kinetic stability of long-lived human lens gamma-crystallins and their isolated double Greek key domains. *Biophys J.* 2019;117:269–280.
43. Mills IA, Flaugh SL, Kosinski-Collins MS, King JA. Folding and stability of the isolated Greek key domains of the long-lived human lens proteins gammaD-crystallin and gammaS-crystallin. *Protein Sci.* 2007;16:2427–2444.
44. Takata T, Smith JP, Arbogast B, David LL, Lampi KJ. Solvent accessibility of betaB2-crystallin and local structural changes due to deamidation at the dimer interface. *Exp Eye Res.* 2010;91:336–346.
45. Kosinski-Collins MS, King J. In vitro unfolding, refolding, and polymerization of human gammaD crystallin, a protein involved in cataract formation. *Protein Sci.* 2003;12:480–490.
46. Hall D, Zhao R, Dehlsen I, et al. Protein aggregate turbidity: Simulation of turbidity profiles for mixed-aggregation reactions. *Anal Biochem.* 2016;498:78–94.
47. Serebryany E, Yu S, Trauger SA, Budnik B, Shakhnovich EI. Dynamic disulfide exchange in a crystallin protein in the human eye lens promotes cataract-associated aggregation. *J Biol Chem.* 2018;293:17997–18009.
48. Quinlan RA, Hogg PJ. γ -Crystallin redox-detox in the lens. *J Biol Chem.* 2018;293:18010–18011.
49. Roskamp KW, Azim S, Kassier G, et al. Human γ S-crystallin-copper binding helps buffer against aggregation caused by oxidative damage. *Biochemistry.* 2020;59:2371–2385.
50. Ciryam P, Kundra R, Morimoto RI, Dobson CM, Vendruscolo M. Supersaturation is a major driving force for protein aggregation in neurodegenerative diseases. *Trends Pharmacol Sci.* 2015;36:72–77.
51. Brubaker WD, Freites JA, Golchert KJ, et al. Separating instability from aggregation propensity in gammaS-crystallin variants. *Biophys J.* 2011;100:498–506.
52. Jung J, Byeon I-JL, Wang Y, King J, Gronenborn AM. The structure of the cataract-causing P23T mutant of human gammaD-crystallin exhibits distinctive local conformational and dynamic changes. *Biochemistry.* 2009;48:2597–2609.
53. Khago D, Wong EK, Kingsley CN, Freites JA, Tobias DJ, Martin RW. Increased hydrophobic surface exposure in the cataract-related G18V variant of human γ S-crystallin. *Biochim Biophys Acta.* 2016;1860:325–332.
54. Kingsley CN, Brubaker WD, Markovic S, et al. Preferential and specific binding of human α B-crystallin to a cataract-related variant of γ S-crystallin. *Structure.* 2013;21:2221–2227.
55. Wintrode PL, Zhang D, Vaidehi N, Arnold FH, Goddard WA 3rd. Protein dynamics in a family of laboratory evolved thermophilic enzymes. *J Mol Biol.* 2003;327:745–757.
56. Takano K, Tsuchimori K, Yamagata Y, Yutani K. Contribution of salt bridges near the surface of a protein to the conformational stability. *Biochemistry.* 2000;39:12375–12381.
57. Strop P, Mayo SL. Contribution of surface salt bridges to protein stability. *Biochemistry.* 2000;39:1251–1255.
58. Zhang K, Zhu X, Lu Y. The proteome of cataract markers: Focus on crystallins. *Adv Clin Chem.* 2018;86:179–210.
59. Skouri-Panet F, Bonneté F, Prat K, Bateman OA, Lubsen NH, Tardieu A. Lens crystallins and oxidation: The special case of gammaS. *Biochim Biophys Acta.* 2001;1524:65–76.
60. Lampi KJ, Fox CB, David LL. Changes in solvent accessibility of wild-type and deamidated betaB2-crystallin following complex formation with alphaA-crystallin. *Exp Eye Res.* 2012;104:48–58.
61. Carver JA, Lindner RA, Lyon C, et al. The interaction of the molecular chaperone alpha-crystallin with unfolding alpha-lactalbumin: A structural and kinetic spectroscopic study. *J Mol Biol.* 2002;318:815–827.
62. Treweek TM, Rekas A, Lindner RA, et al. R120G alphaB-crystallin promotes the unfolding of reduced alpha-lactalbumin and is inherently unstable. *FEBS J.* 2005;272:711–724.
63. Cox D, Selig E, Griffin MDW, Carver JA, Ecroyd H. Small heat-shock proteins prevent α -synuclein aggregation via transient interactions and their efficacy is affected by the rate of aggregation. *J Biol Chem.* 2016;291:22618–22629.
64. Ray NJ, Hall D, Carver JA. A structural and functional study of Gln147 deamidation in alphaA-crystallin, a site of modification in human cataract. *Exp Eye Res.* 2017;161:163–173.
65. Lampi KJ, Wilmarth PA, Murray MR, David LL. Lens beta-crystallins: The role of deamidation and related modifications in aging and cataract. *Prog Biophys Mol Biol.* 2014;115:21–31.
66. Bastrup J, Kastaniegaard K, Asuni AA, Volbracht C, Stensballe A. Proteomic and unbiased post-translational modification profiling of amyloid plaques and surrounding tissue in a transgenic mouse model of Alzheimer's disease. *J Alzheimers Dis.* 2020;73:393–411.
67. Pino LK, Searle BC, Bollinger JG, Nunn B, MacLean B, MacCoss MJ. The skyline ecosystem: Informatics for quantitative mass spectrometry proteomics. *Mass Spectrom Rev.* 2020;39:229–244.

68. Sharma V, Eckels J, Schilling B, et al. Panorama public: A public repository for quantitative data sets processed in skyline. *Mol Cell Proteomics*. 2018;17:1239–1244.

SUPPORTING INFORMATION

Additional supporting information may be found online in the Supporting Information section at the end of this article.

How to cite this article: Vetter CJ, Thorn DC, Wheeler SG, et al. Cumulative deamidations of the major lens protein γ S-crystallin increase its aggregation during unfolding and oxidation. *Protein Science*. 2020;29:1945–1963. <https://doi.org/10.1002/pro.3915>